Article

Effect of Salinity on Hydroxyapatite Nanoparticles Flooding in Enhanced Oil Recovery: A Mechanistic Study

Eugene N. Ngouangna, Mohd Zaidi Jaafar,* Mnam Norddin, Augustine Agi, Faruk Yakasai, Jeffrey O. Oseh, Stanley C. Mamah, Muftahu N. Yahya, and Muhanad Al-Ani

Cite This: ACS Omega 2023, 8, 17819−17833

Read Online

ACCESS | Metrics & More | Article Recommendations

ABSTRACT: Fluid−fluid interactions can affect any enhanced oil recovery (EOR) method, including nanofluid (NF) brine−water flooding. Flooding with NFs changes wettability and lowers oil−water interfacial tension (IFT). Preparation and modification affect the nanoparticle (NP) performance. Hydroxyapatite (HAP) NPs in EOR are yet to be properly verified. HAP was synthesized in this study using co-precipitation and in situ surface functionalization with sodium dodecyl sulfate in order to investigate its impact on EOR processes at high temperatures and different salinities. The following techniques were employed, in that sequence, to verify its synthesis: transmission electron microscopy, zeta potential, thermogravimetric analysis, Fourier transform infrared spectroscopy, X-ray diffraction, particle size analysis, and energy-dispersive X-ray spectra. The outcomes showed the production of HAP, with the particles being evenly dispersed and stable in aqueous solution. The particles' surface charge increased from -5 to -27 mV when the pH was changed from 1 to 13. The HAP NFs at 0.1 wt % altered the wettability of sandstone core plugs from oil-wet at 111.7 to water-wet at 9.0 contact angles at salinity ranges of 5000 ppm to 30,000 ppm. Additionally, the IFT was reduced to 3 mN/m HAP with an incremental oil recovery of 17.9% of the initial oil in place. The HAP NF thus demonstrated excellent effectiveness in EOR through IFT reduction, wettability change, and oil displacement in both low and high salinity conditions.
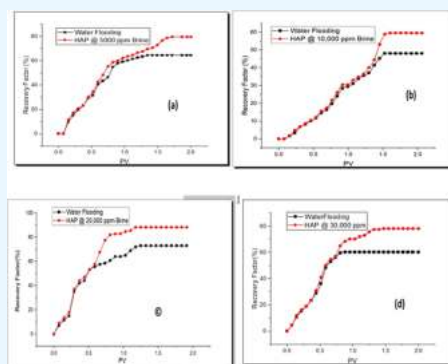
1. INTRODUCTION

Undoubtedly, throughout the last few decades, oil has had a significant impact on the global energy sector and economy.[1] Intense increase in population and industrial activities have led to a sharp increase in energy consumption.[2,3] The present problem is to find a cost-effective way to extract more oil while also delaying the abandonment of oil and gas wells. In most oil reservoirs, a pressure drop that happens during oil production prevents the generation of oil spontaneously.[4−6] In order to increase and improve oil production, numerous techniques have been implemented. These techniques can be divided into three main groups: primary, secondary, and tertiary. The natural energy present in a reservoir drives oil production during the primary stage. Rock and fluid expansion, aquifer drive, solution gas drive, gas cap drive, and gravity segregation are the sources of natural energy. Gas or water injection during the secondary stage boosts natural energy, which in turn improves oil recovery.[7] The amount of initial oil that is still in the reservoir after primary and secondary recovery is greater than 50% on a global scale.[8−11] Oil firms are working extremely hard to increase the oil output by extracting the remaining residual oil utilizing enhanced oil recovery (EOR) methods such chemical flooding (surfactant, polymer, and alkaline.), gas injection, low salinity water flooding, and thermal processes.[12] Innovative approaches are therefore

required in challenging reservoir circumstances where these traditional techniques fail. Several EOR pilot projects have reportedly failed in the literature because of various aspects of the challenging reservoir state. High salinity causes the precipitation of the surfactant. High temperatures cause polymer degradation, which reduces viscosity of the displacing fluid.[13−15]

EOR technologies in hydrocarbon reservoirs include interfacial tension (IFT) reduction,[16] wettability alteration, mobility control, and gravity drainage.[17−19] Due to rising energy demand, oil companies must find new ways to improve oil recovery. NPs are a promising chemical approach in EOR applications.[20] The main EOR mechanisms of nanofluid (NF) flooding, such as wettability modification to more water-wet, IFT reduction, the lowering of oleic phase viscosity, disjoining pressure, and inhibiting asphaltene precipitation, have already been studied in the literature.[21−23] Recent research has thoroughly investigated and reported on the general wettability
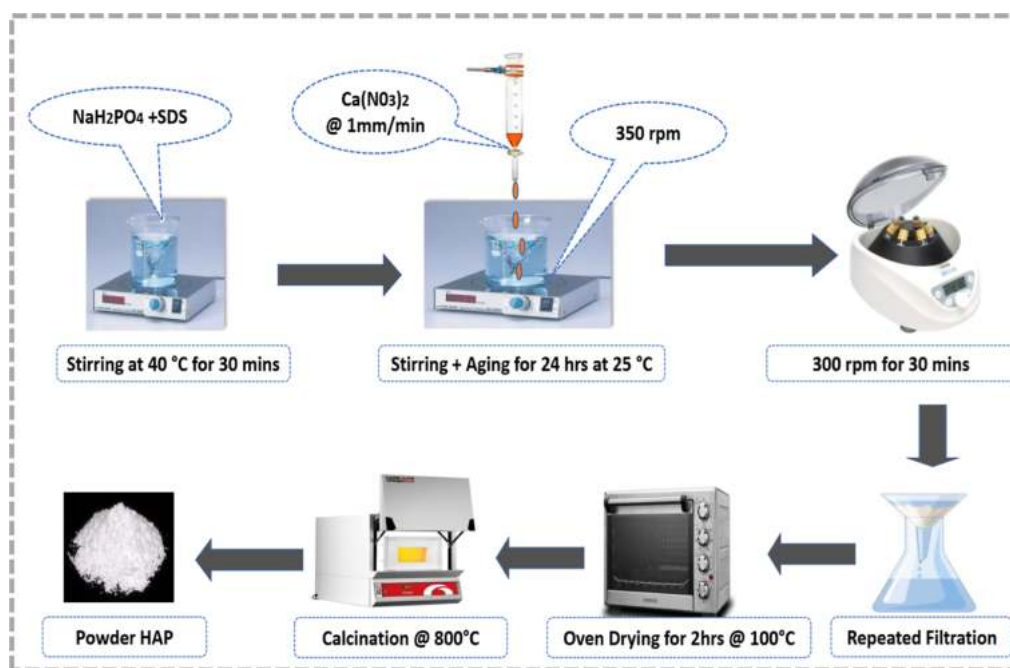
Figure 1. Synthesis and in situ surface modification of HAP using SDS by co-precipitation.

change process. One of the key efficient methods pertaining to EOR is the lowering of IFT between oil and the injected fluid. SiO_2, polymer-coated NPs, ferrofluid, hydrophobic and lipophilic polysilicon NPs, and ferrofluid are some examples of the NPs that have been studied as potential agents to decrease the IFT between the oleic phase and injected fluid into a core or micromodel.

Under high pressure and temperature, NPs are often more resistant to degradation.[24] Due to the development of nanotechnology and the realization of its potential, numerous researchers have investigated the use of NPs to improve oil production in recent years.[7,25−29] Owing to their large-surface area and nanoscale size, NPs have distinct physical and chemical characteristics.[24] It should be observed that there is a wedge film located between the oil drop and the solid surface, and in this film, NPs have a tendency to form more organized structures than they do in the main fluid.[30] This structuring is entropically advantageous because the released water molecules' improved entropy more than makes up for the loss in the ordering region of NPs.[31] The ordered structure is propelled forward by the disjoining pressure generated by the NPs in the wedge film, which is what moves the oil droplet. Brownian motion and electrostatic repulsion between the NPs power this mechanism.[32]

For more than a decade, there has been discussion in the literature on the mechanism of the low salinity EOR process in sandstone reservoirs.[12,33] However, little work has been carried out on high salinity environments. Low salinity water flooding (LSWF) is also used as an EOR technique because water sources are plentiful and affordable.[34] LSWF increases oil recovery through rock/fluid interactions, solution and surface chemistry, and other factors.[35] It is widely accepted that LSWF's EOR is related to wettability adjustment toward more water-wet conditions, which causes positive capillary forces and boosts microscopic sweep efficiency in heterogeneous pore systems.[35−37]

Hydroxyapatite (HAP) nanoparticles (NPs) are used in orthopaedics, maxillofacial surgery, and dentistry to repair or remove hard tissue. Due to the chemical similarity of human bone, mineral components, and dental hard tissues, it has excellent consistency, biocompatibility, and bioactivity. Nano HAP is utilized in bioimaging and therapy. This work addresses this material's neglect in the oil and gas sector particularly in EOR applications. This study examined the impact of HAP surface modified in situ using sodium dodecyl sulfate (SDS) on wettability modification and IFT reduction between brine and oil and oil displacement in sandstone core plugs at various salinities under conditions of high temperature and pressure. The contact angle (CA) was utilized to assess NP-treated sandstone core plug wettability. Second, the IFT between injected fluid and crude oil was accessed, followed by the oil displacement at high temperature and high pressure. Even though most reservoirs run at different ionic strengths, most NP-based EOR tests have been carried out at low salinity levels. This work therefore tests the ability of HAP and NPs in general to displace oil at distinct ionic strengths of electrolytes.

2. MATERIALS AND METHODS

2.1. Materials. The investigation involved the use of the following substances: without further purification, Tayi Scientific Instruments Sdn. Bhd. Malaysia offered SDS, molar mass: 288.372 g/mol, density: 1.01 g/cm^3, calcium nitrate 4-hydrate, molar mass: i288.372 g/mol, melting point: 250 °C, and sodium dihydrogen phosphate (Na_2HPO_4). Crude oil for this project was sourced from Malaysia's Sarawak oil patch. It was a medium-grade crude oil with the following compositions: 73.10 wt % saturates, 19.23 wt % aromatics, 7.48 wt % resins, and 0.19 wt % asphaltenes. It also had a viscosity of i142.68 cP at 27 °C and a 33.3 °API. Merck Group (Sdn. Bhd.), situated in Selangor Malaysia, supplied caustic soda (NaOH)., sodium chloride (NaCl), and hydrochloric acid (HCl) and cores of sandstone taken from the Malaysian oil sector of Sarawak.

2.2. Methods. *2.2.1. Synthesis of HAP.* Before usage, all equipment was thoroughly cleaned with distilled water to remove any contaminants. Figure 1 provides more details about the experimental setup (2). Using a measuring cylinder, 200 mL of 0.06 M Na_2HPO_{4ii} and 200 mL of SDS were added to a 1 L beaker to prepare the solution. The mixture was heated for 30 min at 60 °C while being stirred with a magnetic stirrer running at 350 rpm. Using a graduated burette, 20 mL of 0.1 M $Ca(NO_3)_{2i}$ solution was introduced into the mixture while being continuously stirred at 350 rpm (Figure 1). The use of aqueous solutions of HCl or NaOH allowed the pH of the solution to be changed and kept at 9.0. To guarantee full precipitation, the solution was aged for 24 h at 25 °C while being constantly stirred. After 30 min of centrifugation at 300 rpm, the precipitate was repeatedly filtered using the filter paper, washed with distilled water, and dried in an oven for 2 h at 100 °C. To produce powder HAP, the sample was calcined at 800 °C for 3 h in a furnace followed by crushing. In order to assure accuracy, the experiment was repeated. The controlled precipitation was used to synthesize HAP according to the following scheme

$$10Ca(NO_3)_2 \cdot 4H_2O + 6Na_2HPO_4 + 8NaOH$$

$$\rightarrow Ca_{10}(PO_4)_6(OH)_2 + 20NaNO_3 + 46H_2O \quad (1)$$
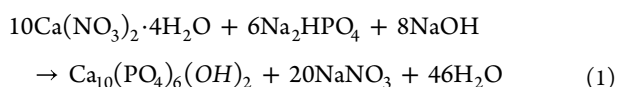
2.2.2. Characterization. The shape, particle size, and elemental constitution of HAP were investigated using HITACHI (model: HT 7700) 120 kV high-resolution transmission electron microscopy (HRTEM)i with energy-dispersive X-ray (EDX). A Shimadzu IR Tracer-100 (Fourier transform infrared spectroscope) FTIR with a scanning range of 370 to 4000 cm^{-1} was used to analyze the functional groups of the NPs. The surface charge and zeta potential (ZP) with the average hydrodynamic diameters of HAP were measured using a light scattering instrument (Malvern Instruments, serial number: MAL1098100, Zetasizer Ver. 7.11). After the HAP had been dissolved in deionized water and sonicated for 10 min, the analysis was carried out in an omega cuvette. The pH range was changed, the count rate was 241.5 (kcps), and the temperature was 25 °C. The thermogravimetric analysis (TGA) of the particles was accessed using a Universal V4.5A TA Instrument. Finally, the crystallography of the material was analyzed using X-ray 40 kV, 30 mA at 8.2551 °/min.

2.2.3. Fluid Preparation. Brine solution with a range of 5000 to 30,000 ppm was used to produce NFs with concentrations between 0.05 and 0.1 wt %. The ideal NF concentration as indicated in the literature served as the basis for choosing this concentration range. Concentrations more than 0.1 wt % run the risk of obstructing pore channels, causing fast aggregation, harming the formation, and impairing permeability in a beaker, the dried NPs were collected, weighed, and combined with a brine solution. After that, the mixture was heated to 28 °C and agitated with a magnetic stirrer for 5 min. To lessen agglomeration, the created solution was subsequently homogenized for 15 min in a Branson iDHA-1000-E, i100 W, 40 kHz, Danbury, ultrasonic bath.

2.2.4. CA Measurements. CA measurements were carried out in order to investigate the possibility of NFs influencing rock wettability using the sessile drop technique. The CA between a water droplet and the surface of the rock is calculated when the droplet is placed on the core sample. For the purpose of examining wettability changes after oil saturation, CA measurements were performed before and after treatment with the NFs. Each saturated core sample underwent a number of NF

treatments, ranging from 0.1 wt %. 5000 to 30,000 parts per million (ppm) of brine, and 80 °C temperature. The temperature was limited at 80 °C due to the limitation of the equipment used. Before performing the CA measurements, sandstone cores were repeatedly washed with toluene and acetone and allowed to dry in an oven at 100 °C for 24 h and then allowed to cool. To ensure that the oil was fully absorbed, they were then aged in crude oil for 48 h, cleaned, and the CA measured. The cores were aged in NFs for a second time for a total of 48 h to assure wettability alteration and then heated at 100 °C to mimic the reservoir temperature before the C A measurement was repeated.

2.2.5. IFT Measurements. The Wilhelmy Plate method was used to determine the IFT between crude oil and NFs. The measurement method included cleaning the platinum plate with acetone and a hot flame to ensure it was pollutant-free, measuring the force required to pull the plate out of the dense phase after submerging it 3 mm into the aqueous phase, adding oil without causing the aqueous phase to be distressed. The testing involved varying temperature (80 °C), brine concentration (5000−30,000 ppm), and particle concentration (0.05−0.1 wt %). At 26 °C under atmospheric pressure, distilled water's surface tension (SFT) was calculated to be 71.84 mN/mi. To assure accuracy, each data point was examined three times, with the average outcome being noted.

2.2.6. Core Sample Preparation Prior to Flooding. HAP NF oil displacement tests were carried out using mid-permeability sandstone cores (Figure 2) with the properties listed in Table 1.

Figure 2. Sandstone core samples for oil displacement.

Table 1. Sandstone Core Properties Prior to Oil Displacement

core	length (cm)	diameter (cm)	porosity (%)	permeability (mD)
C_1	7.1	3.5	22.3	275.001
C_2	7.6	3.6	21.2	243.369
C_3	7.0	3.5	23.5	274.697
C_4	7.4	3.5	25.3	395.101

Because the four mid-permeability sandstone cores are from the same outcrop, their properties are identical. To remove impurities from the cores, they are washed in a Soxhlet extractor with toluene and acetone. The cores were then dried in an oven at 100 °C for 48 h. Subsequently, the cores were weighed using a mass balance to determine their dry weight. The porosity, pore volume, and bulk volume were then calculated using a TPI-219 Porosimeter at 25 °C and under atmospheric pressure. The permeabilities of the cores were then determined using a VINCI Liquid Perm at 25 °C and atmospheric pressure, and the results were recorded. The cores were then saturated with brine and pressurized at 2000 psi for 24 h prior to the oil recovery tests to ensure complete saturation.

2.2.7. Oil Displacement Analysis. Prior to the oil recovery measurements, the bulk volume was determined by taking core measurements with the use of a caliper, while the pore volume
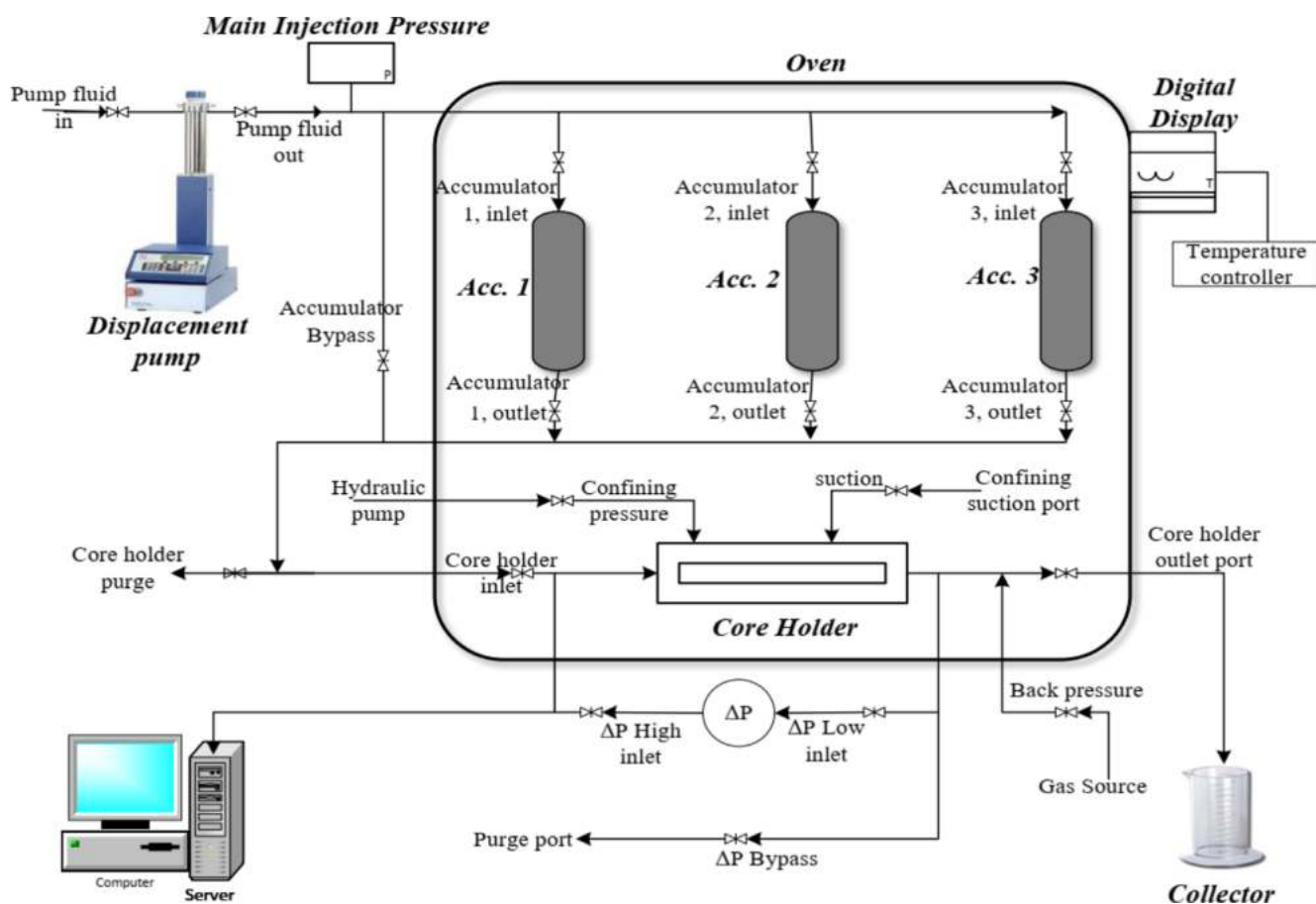
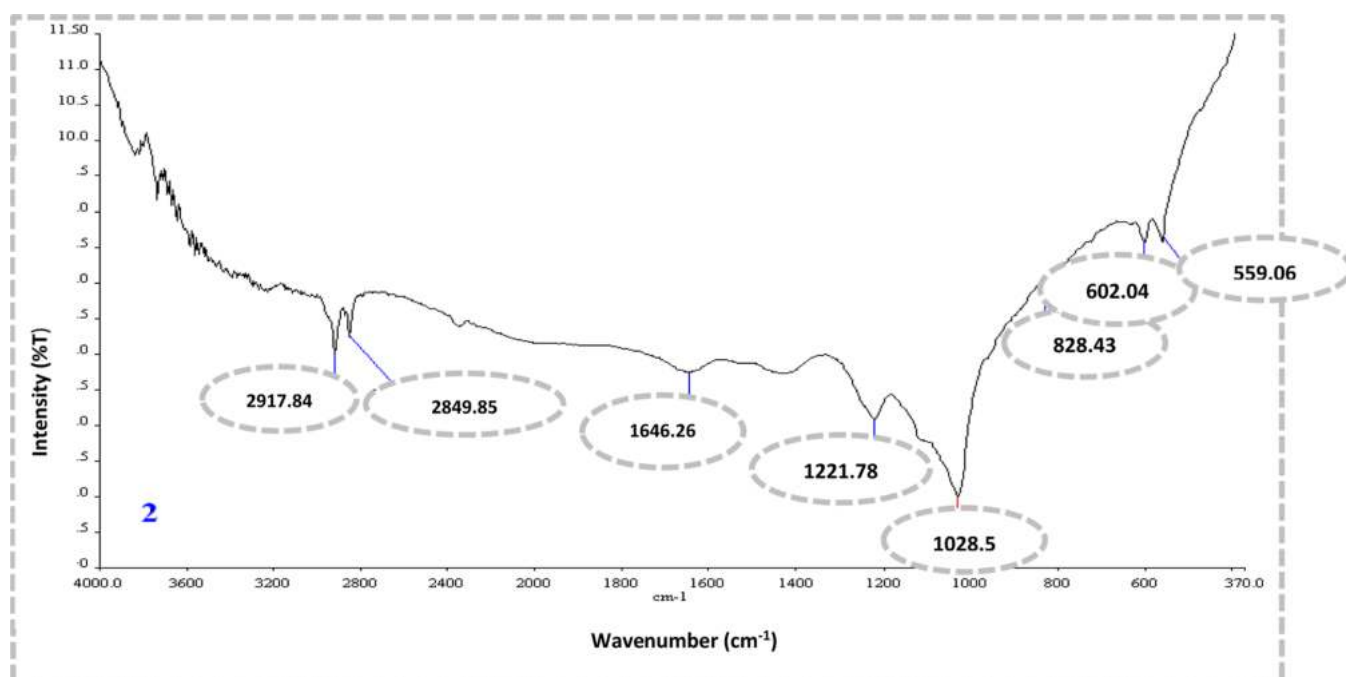**Figure 3.** Fars EOR technologies' HTHP setup.

Figure 4. FTIR spectrum.

was determined by using a helium porosimeter (TPI-219). The apparatus measures pore volume using billets and Boyle's law principles. Permeability measurements were taken before and after NF flooding with a liquid permeameter (Vinci technologies), and permeability was calculated using Darcy's law (eq. 2). To pass brine through the core, carbo dioxide was used. The differential pressure measurements were taken from the apparatus, and a stop watch was used to check how long it
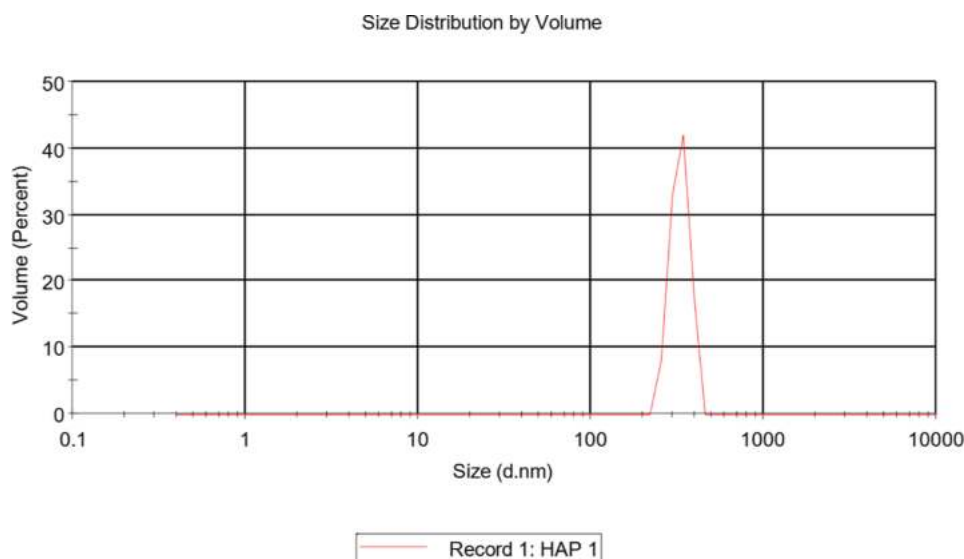
Size Distribution by Volume
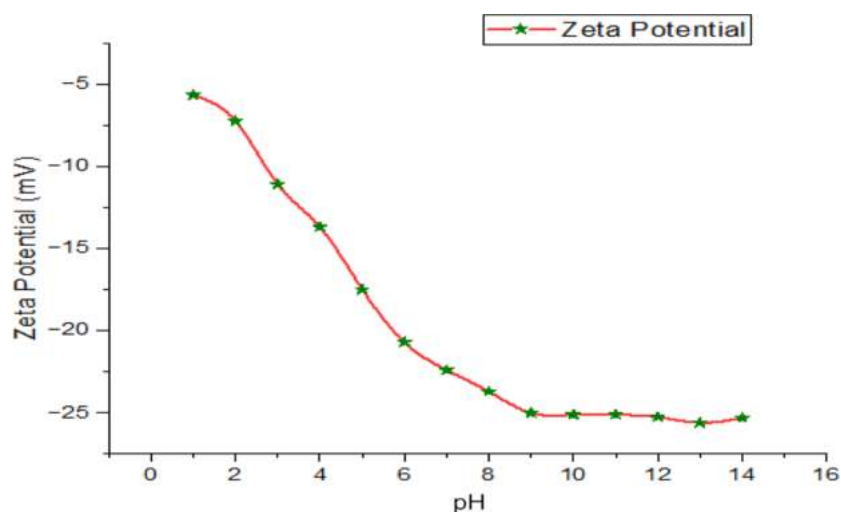

Figure 5. Particle size distribution.

Figure 6. Zeta potential results.

took to collect 100, 50, and 10 mL brine solution to calculate the flow rate. The core samples and their characteristics are detailed in Figure 2 and Table 2.

$$Q = K{\cdot}A\frac{(P1 - P2)}{\mu{\cdot}L} \tag{2}$$

where Q is the flow rate (mL/min), K is the core's absolute permeability (mD), L is its length (cm), A is its surface area (cm^2), μ is water's dynamic viscosity (mPa·s), P_1 is the inlet pressure (psi), and P_2 is the outlet pressure (psi), respectively.

Fars EOR Technologies' high-temperature high-pressure (HTHP) equipment was used for the core flooding experiments. An oven and a hydraulic pump are used to regulate temperature and confining pressure, respectively. Three piston-like accumulators and a core holder allow the system to perform different injection configurations. The equipment was linked to a Teledyne ISCO pump to pump injectants from the accumulator through the core. Figure 3 depicts the experimental setup schematically. The instrument was cleaned before each oil displacement experiment, and the accumulators were filled with brine, oil, and NFs. The injection fluid flow rate was set to 0.4

mL/min, the oven temperature to 80 °C, and the confining pressure was set to 1800 psi. 2 PV of oil was injected into each core to displace the initial brine and saturate it with oil; the water collected was used to calculate the original oil in place (OOIP) and connate water. To achieve equilibrium, the system was aged for 24i h. Brine solution (5000 ppm) was injected until water breakthrough at 1.0 PV for waterflooding. Injection, however, continued until 2 PV. Following that, NFs were injected into the effluent until the oil-cut was less than 1%. This varied between 1.1 and 1.4 PV. As a result, all NFs were injected until 2 PV to ensure consistency. Following that, 1.0 PV of chase water was injected into the cores to flush the NPs and determine the total oil recovery.

3. RESULTS AND DISCUSSION

3.1. Fourier Transform Infrared Spectroscopy. The chemical characteristics of powder samples can be ascertained using the FTIR technique. The two most distinguishable functional groups in the generated HAP's FTIR spectrum are the phosphate $(PO_4{}^{3-})$ and hydroxyl (OH^-) groups. Figure 4 displays the outcomes of the analysis of the HAP FTIR
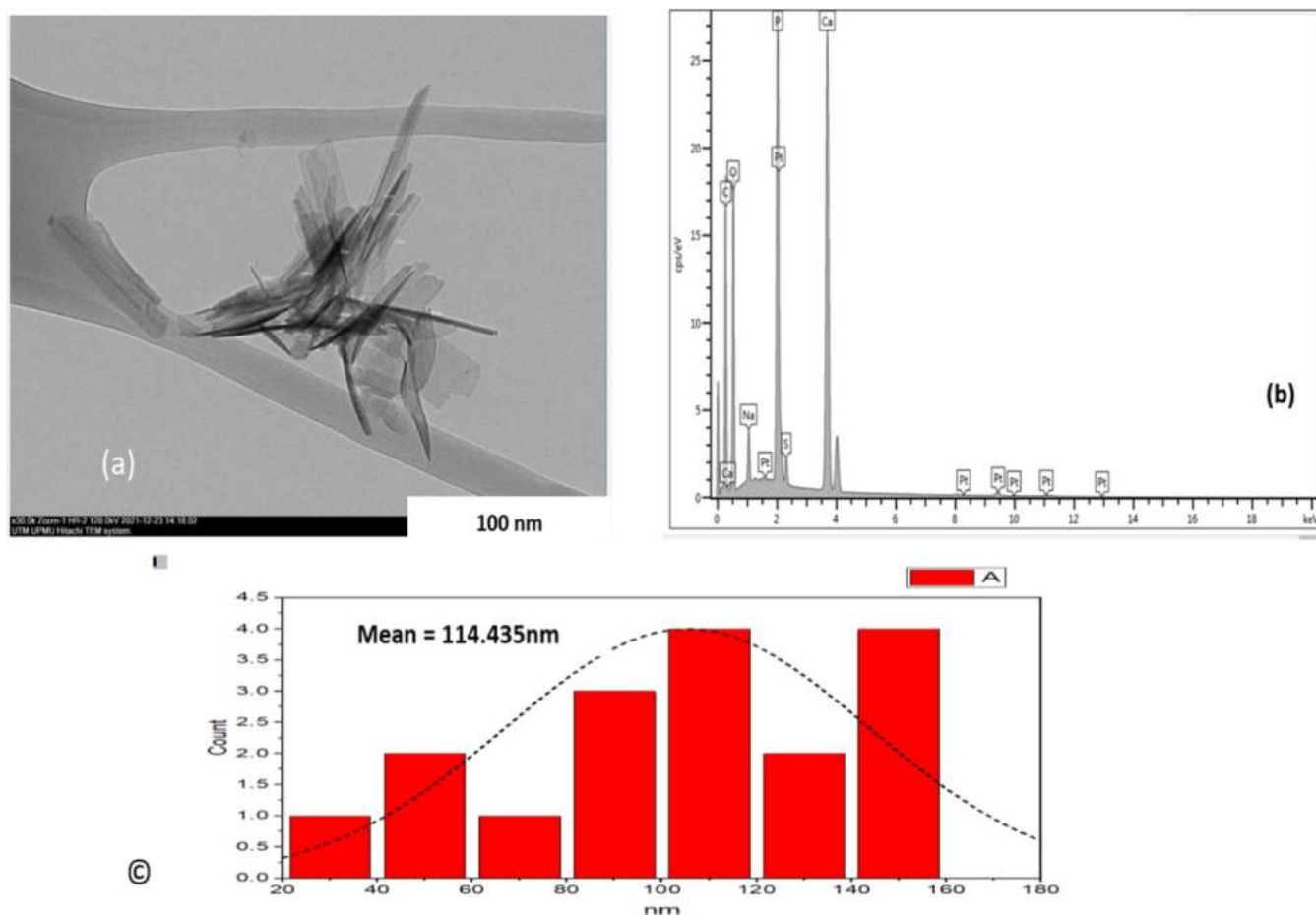
Figure 7. TEM results with (a) HAP morphology, (b) elemental composition, and (c) size distribution.

spectrum. The hydroxyl group stretching modes of adsorbed water molecules on HAP are linked to the bands at 2849.85 and 2917.84 cm^{-1}. These results demonstrated that a considerable number of structural OH^{-i} groups and a small number of water molecules from the aqueous solution were adsorbed onto the surface of HAP. The (P−O) bond's symmetric stretching mode is represented by the 1028.5 band, while its asymmetric bending mode is represented by the 602.04 and 559.60 bands.[37,38]

3.2. Particle Size Analysis. The Malvern Zeta Sizer version 7.11i was used to assess the distribution of HAP. The outcomes illustrate that the particles are mostly nanosized, ranging from 250i to 400 nm, with only a few micrometer-sized particles. The particles' average hydrodynamic diameter, 323.5 nm (Figure 5), indicates that they are in the nanometer range and are suitable for application in EOR.[39] The particles are larger as compared to the TEMii analysis, which could be ascribed to two factors: either growth, caused by water molecules absorption on the surface of the NPs during dispersion in water,[24,40] or agglomeration.[39,41]

3.3. Zeta Potential. The most popular stabilization test used to evaluate the dispersion stability of compounded NFs is sedimentation.[9,42] However, this method is time-consuming and provides insignificant findings, making it ineffective for assessing HAP dispersion stability. ZP measurements were carried out to quantify the surface charge in order to examine the stability of the produced NFs in terms of dispersion. ZP as a function of pH was calculated using a Malvern Zeta Sizer version 7.11i. The pH range at which the greatest number of hydroxyl ions are dispersed on the surface of the HAP was determined (Figure 6).

The HAP positive charges could be neutralized and replaced with negative SDS ions by the SDS attachment at a pH of 1.69 (acidic). The findings demonstrate that the ZP ranges from −5.69 to −27.2 mV between pH values of 1.69 to 12.8, showing that the particles are more stable in basic media.[43] ZP values of NFs less than 5 (5.0 mV) indicate unstable suspensions, which are most likely caused by agglomeration.[44] The average ZP value indicates that the in situ-modified HAPs are extremely stable. The magnitude reveals the colloidal system's potential stability. The particles in suspension resist one another and have no propensity to stick together if all of them have a strong negative or positive ZP. HAP demonstrates long-term fluid stability and can therefore be advised for EOR applications based on its colloidal stability and dispersion with a ZP of −27.2 mV.[45] During synthesis, the pH was adjusted and kept constant at 9.0 throughout the process. However, during ZP measurements, the ZP value at this pH was −25 mV. Therefore, the −27.2 mV obtained at pH. 14 indicates that the ZP does not change much after its original state. Even though, it tends to drop more in the acidic medium.

3.4. Surface Morphology, Size Distribution, and Elemental Composition. The order in which the components are mixed heavily influences the composition, shape, and size of NPs produced in the presence of a surfactant. According to the steps outlined in Section 2, a Na$_2$HPO$_4$ solution was added to a reactor that already contained an SDS solution with a concentration of 0.5 M. This approach generated rodlike particles with crystalline structures with lengths ranging from 20 to 140 nm and a mean length of 104.3 nm.[46,47] According to the
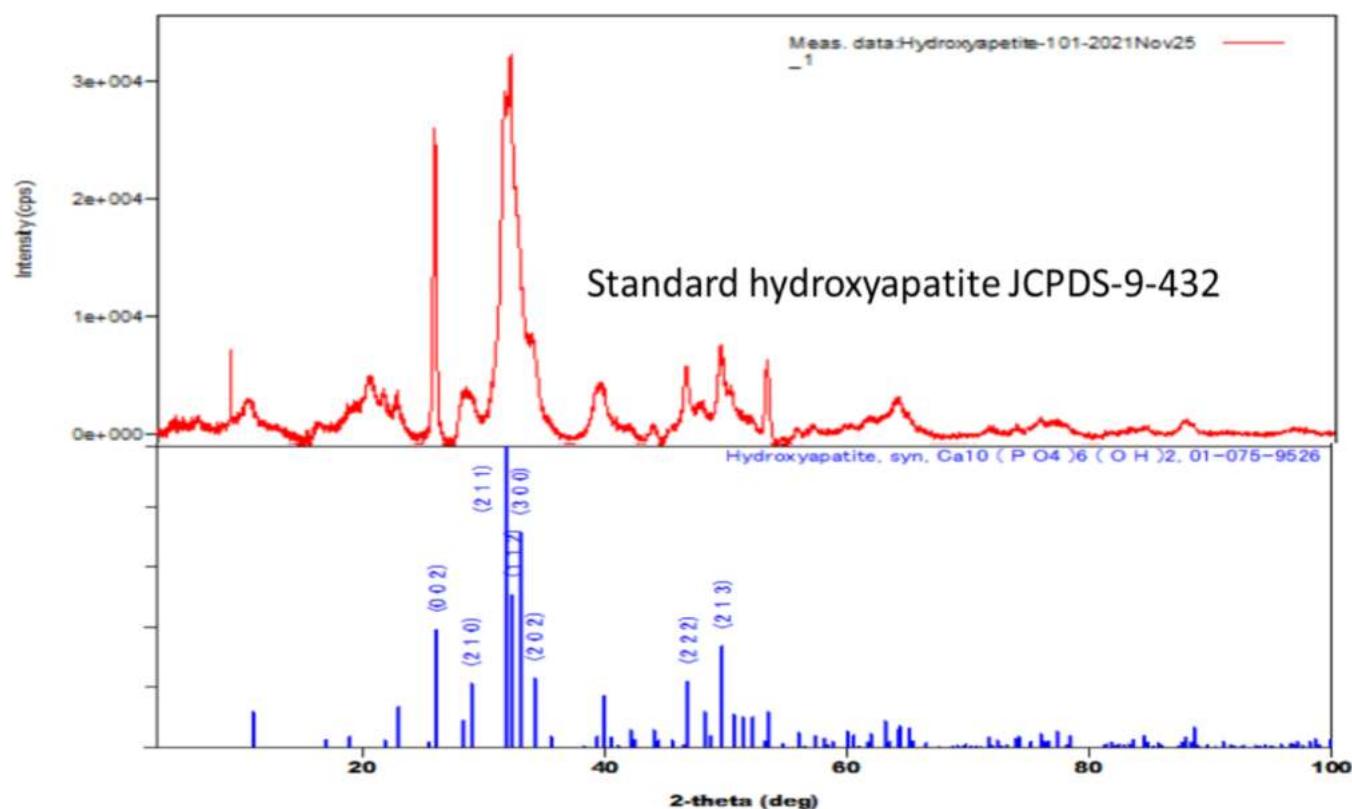
Figure 8. XRD results.

HR-TEMi picture (Figure 7a), the NPs' diameters ranged from 5 to 15 nm. Using image-J software, the NP lengths were measured, and the distribution was examined using origin software (Figure 7 c). The presence of P, Ca, and O, all of which are assigned to HAP and support its synthesis, is shown in the elemental composition of the EDX spectrum (Figure 7b). Since the calculated Ca/Pi ratio from the EDX result is 1.69 and less than 2, it is within the permitted range of HAP values, consequently, the computed Ca/P molar ratio from the elemental composition is acceptable. There should be a 1.67 standard HAP ratio between calcium and phosphorus.[48,49] Since the reservoir pores are in the micrometer range, the diameters (rod lengths) of NPs are within the range of conventional NP sizes employed in EOR applications. As a result, this proves that HAP is appropriate for EOR applications.

3.5. X-ray Diffraction Characterization. Powder X-ray diffraction (XRD) was used to do structural investigation on the sample. Figure 8 illustrates the HAP's XRD patterns. Sharper peaks in the pattern imply improved crystallinity. Good agreement between the peak positions and the JCPDS can be found (09432).[46] As can be observed, the hexagonal system with primitive lattice perfectly matches the HAP XRD patterns with the diffraction peaks produced at 2.82, 2.79, and 2.72 and the other d-spacing values. The findings of the present investigation's XRD analysis are in good accordance with the findings that have been published.[50] No additional secondary phases, such as calcite, were detected; the peaks were exclusively crystalline in structure and comprised the hexagonal HAP phase.[51] The large peaks around peak numbers (002) and (211) indicate that the crystallite size was on the order of a nanometer scale.[51] However, due to peak broadening, the peaks that represent the (112), (300), and (202) reflections are overlapped. This suggests that crystallinity and crystal size may have

decreased, and the decrease could be attributed to the presence of dihydrogen phosphate.[52]

3.6. Thermogravimetric Analysis. The number and kind of impurities present, the heating environment, additives, and other parameters including sample size, particle size, and heating rate of the sample have all been observed to alter the structure of HAP heated at high temperatures.[53] Thermal breakdown of the powder was used to test the thermal stability of the HAP sample. According to the TGA data given in Figure 9, it was found that the elimination of absorbed water caused the HAP sample to decompose marginally below 200 °C. However, the degradation of the organic residue component may be the primary cause of decomposition between 200 and 380 °C,[54] after which the material was stable till 800 °C. The TGA curve demonstrates that the thermal decomposition of the HAP sample occurred with an endothermic peak at 100, 200, and 250 °C, and that this peak was solely caused by the degradation of the remaining water in the gel. Most reservoirs operate at temperatures between 90 and 120 °C.[55] However, HAP could still withstand decomposition at 800 °C, making it a remarkable chemical for EOR.

3.7. IFT Analysis. In order to quantify the ideal HAP concentration, which was subsequently maintained in the succeeding tests, the SFT of distilled with different concentrations of HAP was first measured (Figure 10) prior to the IFT analysis. From the SFT results, the optimum concentration of HAP was 0.1 wt % at 31.6 mN/m. This concentration was maintained in the IFT analysis and subsequent tests. IFT is a key statistic in EOR processes because it measures the energy at the interface of immiscible fluids. Successful EOR chemicals that decrease the IFT between the oil and the displacing fluid include surfactants, polymers, NPs, and low brine. Oil droplets that have been trapped deform and spread easily across the porous media
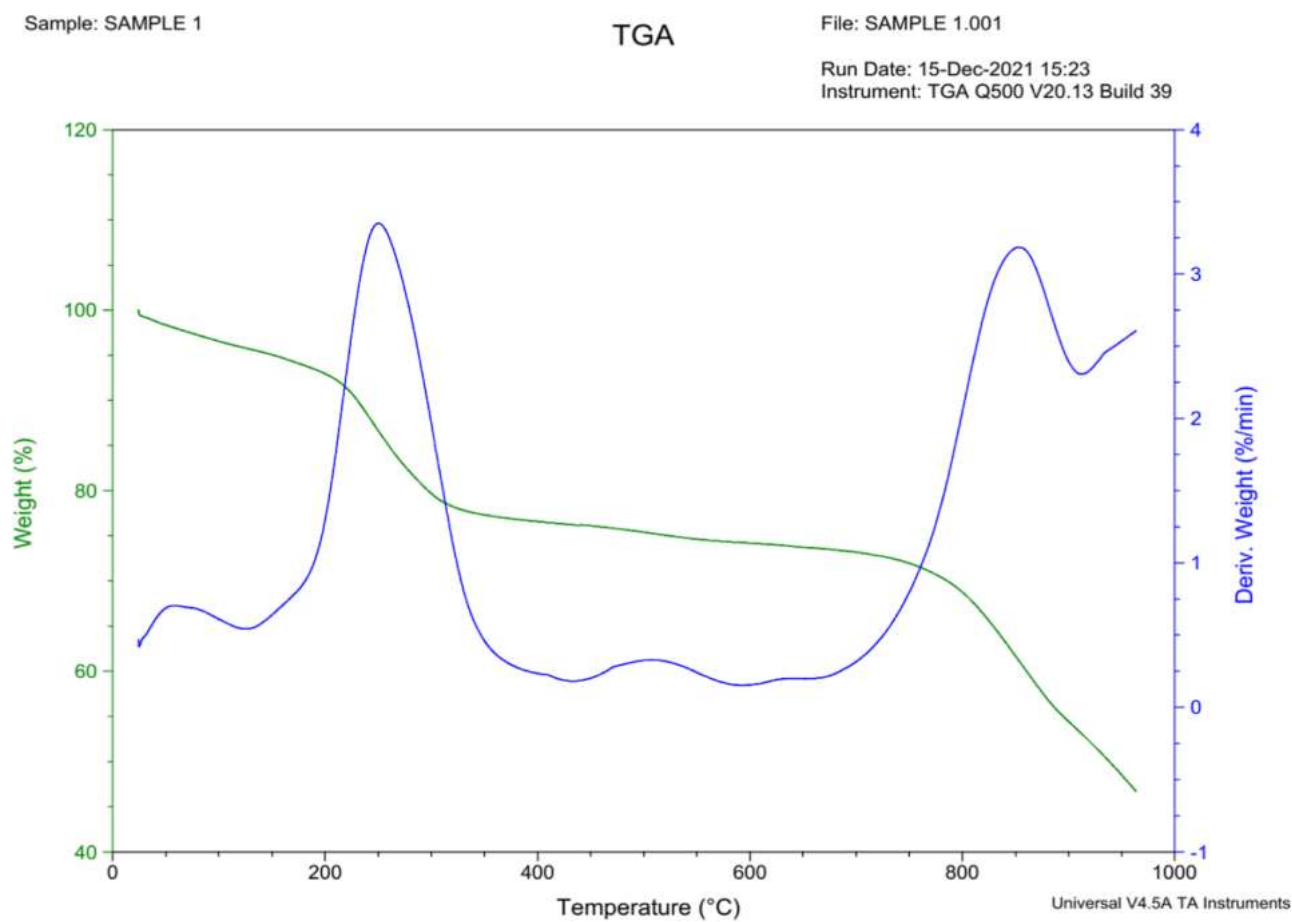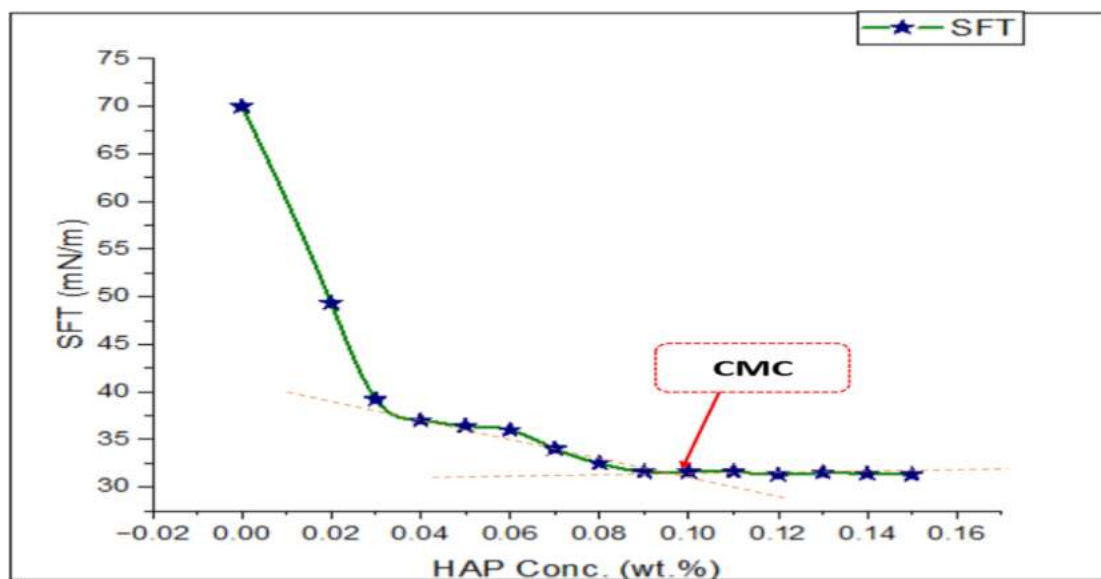
Figure 9. TGA results.

Figure 10. SFT results and critical micelle concentration.

when the IFT between oil and water drops. Some of the factors that might have an impact on IFT include temperature, NP concentration, oil composition, brine concentration, and NP surface energy. Therefore, the effect of salinity on the IFT process of the HAP was examined in this section. Figure 10 illustrates the impact of HAP at salinities of 5000, 10,000, 20,000, and 30,000 ppm on the IFT of the oleic−aqueous

interface. The IFT of the oil−HAP solutions decreased in the presence of brine to a reasonably average value of 3.0 mN/m (Figure 11), which is comparable to that reported in the literature. When NaCl is present, the oil begins to fairly dissolve. This value was achieved at 30,000 ppm. This is followed by the amphiphilic compound sorbing at the interface, which further reduces the IFT.[56] The electrical double layer (EDL)
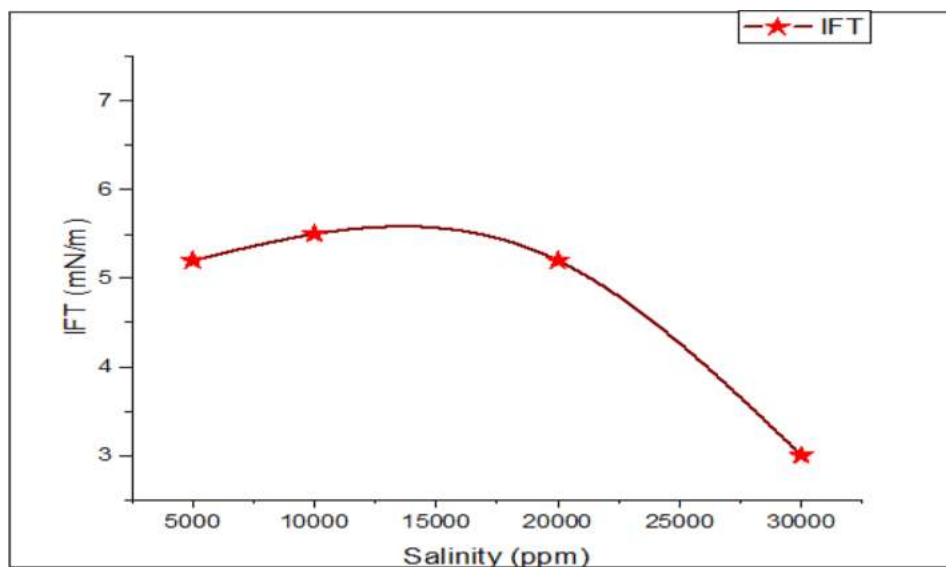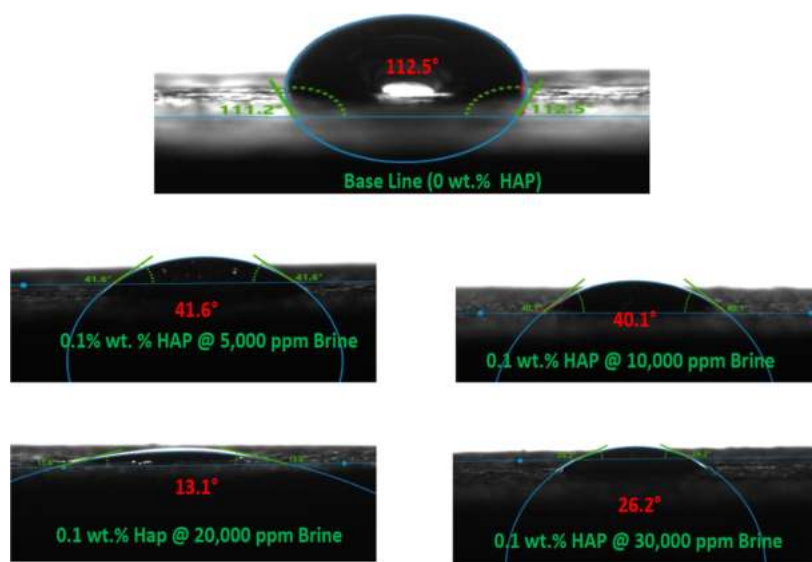
Figure 11. IFT results.

Figure 12. Contact results at various varied salinities.

surrounding the NP at the oil−HAP NF interface is compressed by the brine, which accounts for the low value of IFT. As a result, there is less attraction between adsorbed NPs at the interface. Consequently, a greater IFT reduction results from an increase in the adsorption rate of the surface-active NPs at the interface.[57] The capacity of surfactants to lower IFT to extremely low values is also well documented. The 3 mN/m (Figure 11) IFT recorded is not only attributed to salinity and HAP concentration but the influence of SDS equally contributes significantly. Surfactants have repeatedly been reported to have shown IFT values below 1 mN/m.[58,59] This confirms that the reported 3 mN/m IFT achieved in this research is strongly influenced by the presence of SDS.

The electrolyte interferes with particle surface characteristics and positioning at the oil−water interface. Consequently, some researchers have discovered that they significantly aid in the decrease of IFT,[60,61] while others have discovered utterly different tendencies.[22,62,63] We measured the equilibrium IFT values for 0.1 wt % HAP-NP concentration at various electrolytes (5000, 10,000, 20,000, and 30,000 ppm), respectively, at 80 °Ci to mimic the reservoir temperature. The IFT decreased steadily as the NaCl level increased. This is due to the EDL created when the salt ions come in contact with negatively charged NPs.[39] The sodium and chloride ions in the bulk aqueous phase are stable and do not approach the oil−water contact at very low NaCl concentrations (5000 ppm), allowing the structure of water at the interface to remain the same. As the NaCl concentration rises, the ions get closer to the oil−water interface.[64] Because there is more contact between the NPs and the aqueous solution when NaCl is added, the IFT decreases.[63] The partly negative charge of the NPs interacts more easily with the sodium cation (Na$^+$). The negative charges on the surface of HAP are screened by the opposite charge of Na$^+$. This lessens the thickness of the double layer, increasing the density of NPs at the interface and decreasing the IFT. Cl$^-$ ions, on the other hand, are assumed to adsorb to the oil−water interface and are present in the double layer as counterions.
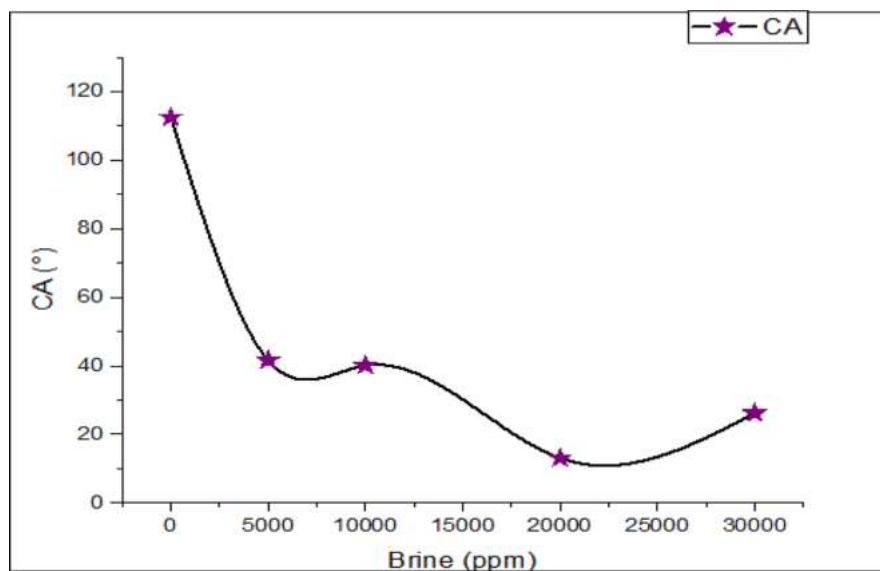
Figure 13. Contact angle variation at various brine concentrations.

As more NPs are adsorbing at the contact, the IFT decreases.[65] Salt therefore reduces the IFT at the oil−water contact, demonstrating that as ionic strength rises, so does the number of particles at the interface. Salt micro-clusters cause fewer free ions to screen electrostatic interactions, which increases repulsion in smooth NPs. Additionally, charged surfaces with high ionic strengths have a short-range repulsion known as hydration force, which, depending on the surface, can be oscillatory or repulsive. Polarization caused by the dielectric contrast between dielectric surfaces and water produces oscillatory ionic profiles in slabs when volume effects that were previously disregarded are taken into account. When the NP charge is expected to be very slightly affected by polarization effects, condensed ions can cause steric repulsion.[66] IFT is lowered as a result of the clusters staying at the oil−water interface, being larger than individual NPs, and being adsorbed there.

3.8. Wettability Analysis. To reduce oil capillary entrapment, boost water absorption, and boost oil counter-current output, any rock's wettability can switch from being oil-wet to water-wet. The natural water wetness of the rock may vary if the water layer that separates crude oil from the mineral surface is disturbed because it is not always permanent. Because of this, the aqueous film's wettability must be changed in order to destabilize and burst the disjoining pressure. CA, which can reveal information on how reservoir rocks wet, was used to evaluate the wettability modification of sandstone cores. Rocks that are oil-wet have a CA greater than 110°, rocks that are water-wet have a CA lower than 70°, and rocks that are intermediately wet have a CA that is between 110 and 70°.[67] Due to its higher precision than optical methods, use of a sensitive microbalance, enhanced reproducibility due to the wide scanning area of substrates, and precise measurement of the dynamic effect during wetting, the bubble drop method was utilized prior to the CA measurements. The effect of HAP NF on wettability was investigated in this report as a function of salinity (Figure 12).

It is well known that salt concentrations in oil reserves are often rather high. A fluid's salinity has a big impact on its characteristics. Therefore, it is crucial to look into how HAP NFs perform in various salinity settings. According to CA tests

contrasting crude oil and oil-wet sandstone core substrates aged in the base fluid, the lowest CA measured corresponds to the 20,000 ppm brine solution. However, the CA value only slightly rises with salinity above this optimal salinity (20,000 ppm) (Figure 13). The outcome is in line with that on functionalized iron-carbon nanohybrids.[7] It is possible that NP adherence and oil dissolution were made easier by the electrostatic interactions between NA$^+$, Cl$^-$, and the surface of the sandstone. Consequently, the wettability change in low salinity concentrations is enhanced.[20] The oppositely charged anions and cations of NaCl reduced the electrostatic repulsive forces of the NPs, which resulted in a lower disjoining pressure and rapid aggregation and sedimentation. As a result, NPs and sandstone cores interact less frequently and with less dispersion (3000 ppm).[68] This is consistent with research showing that the disjoining pressure rises with the intensity of the electrostatic forces and that the thickness and expansion of the EDL have a dominant influence on the detachment of oil from the rock surface.[20] It is significant to remember that even at high NaCl concentrations, all of the NFs have a strong capacity to change the wettability of sandstone surfaces into a water-wet state. This study suggests that HAP has a substantial potential for use in EOR where high salinities are common. The key factor in wettability change processes is the generated attractive and repulsive forces at brine/rock and oil/brine interfaces.[32] This is related to the impacts of salting in and out, the development of the EDL, and the ion exchange between clay minerals and salinity water.[69,70] Therefore, when the ion concentration in the injected brine grows, the hydrogen bonds between water molecules and the hydrophobic components of the organic materials may be broken, reducing their solubility in the aqueous phase.[71] The degree of rock wettability alteration is decreased as a result of this occurrence, known as the salting out effect.[72] On the other hand, during the salting in process, the solubility of organic molecules in the aqueous phase increases with decreasing salinity.[73] Increase in polar organic hydrocarbon detachment from the surface of rocks and an increase in the solubility of organic materials in water work together to advance the wettability of rocks toward a water-wet condition.[68] Furthermore, the wettability alteration process and interactions at the oil−brine interface are mostly caused by salting out and
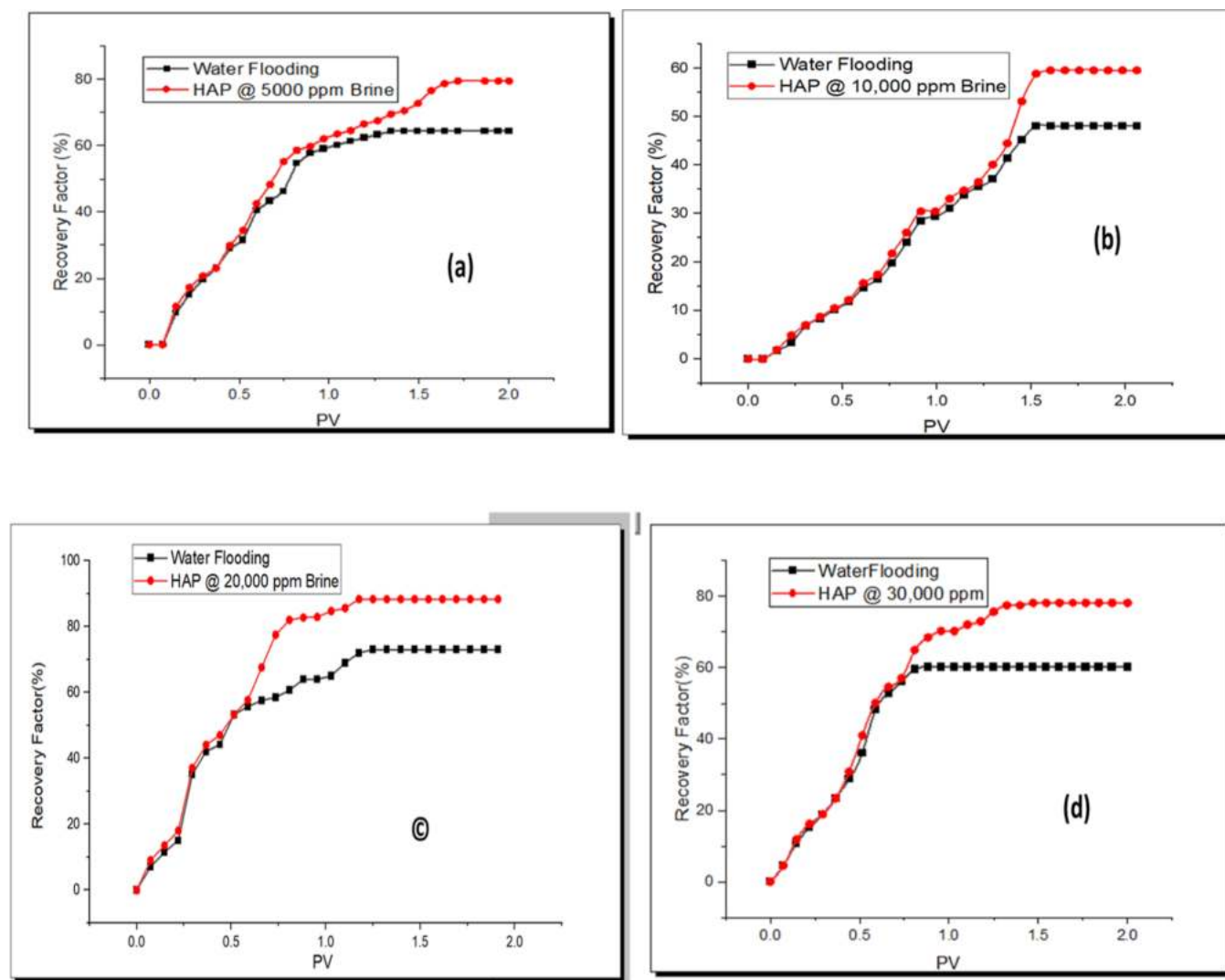
Figure 14. Oil displacement results at brine concentrations of (a) 5000, (b) 10,000, (c) 20,000, and (d) 30,000 ppm.

salting in mechanisms. The other potential element affecting rock wettability is the growth of the EDL as a result of repulsive forces playing a dominant role at contacts between brine, rock, and oil, where this mechanism is most active.[70] As a result, an ionic excess layer is created when an electrolyte solution, such as brine, is exposed to a polar surface due to particle ionizations, ionic dissolution, and ion adsorption.[6,74,75] Thermal and Brownian movements within this layer create an EDL in which co-ions are repelled and counterions are drawn to the charged surfaces and hence a reduction in CA.

3.9. Oil Displacement Analysis. Prior to the oil displacement test, four mid-permeability sandstone cores (Table 2) were used with HAP NF at varied ionic strengths. Core C_1 was employed for 5000 ppm, C_2 for 10,000 ppm, C_3 for 20,000 ppm, and C_4 for 30,000 ppm, respectively. Since the four mid-permeability sandstone cores come from different outcrops but the same field, their characteristics vary slightly. High pressure (1800 psi), high temperature (80 °C), and saline brine solutions of various concentrations were used in the experiment to simulate the HPHT reservoir. Following the procedure of flooding with water, HAP NF was flooded subsequently. Temperature, pressure, flow rate, and injected pore volume were kept constant for all flooding operations to allow for

appropriate comparison. A function of the injected pore volume was used to display the cumulative oil recovery. In accordance with the guidelines for NP field injection for EOR operations, the HAP concentration was set at 0.1 wt %.

The cumulative oil recovery vs pore volume plot of HAP NF is shown in Figure 14. From the OOIP, the waterflooding operation retrieved a large amount of oil. Then, as a tertiary procedure for oil recovery, chemical floods with 0.1 wt % concentrations of HAP NF were independently studied. HAP improved oil recovery during the flooding process with an incremental oil recovery of 6.3% for 5000 ppm brine concentration, 11.5% for 10,000 ppm, 15.3% for 20,000 ppm, and 17.9% for 30,000 ppm, respectively. The incremental oil recovery (Figure 15 and Table 2) increased from 5000 to 30,000 ppm. This is consistent with the findings from the IFT and wettability tests.

According to the IFT evaluation experiment, the NF had a high interfacial activity due to its significant decrease between oil and brine. This alone is therefore an outstanding potential for oil recovery. The improved oil recovery could equally be attributed to the HAP NF's capacity to change the rock surface wettability between brine and oil, which makes it easier for oil droplets to be removed from solid surfaces. Additionally, the tightly packed
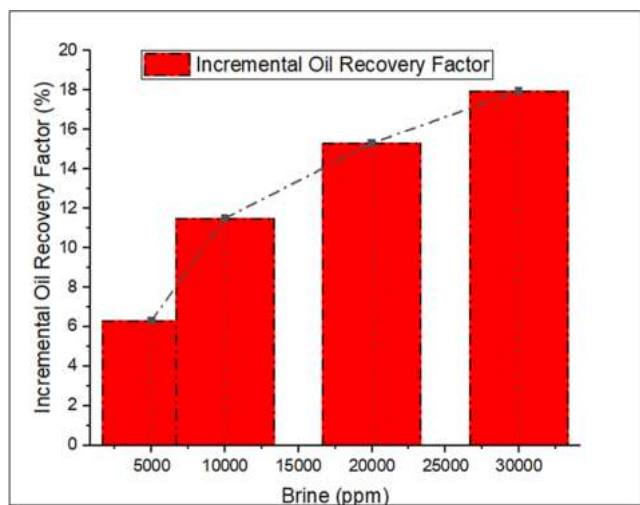
Figure 15. Incremental oil recovery as a function of brine concentrations.

Figure 16. Differential pressure.

NPs at the water/oil interface may create an interface film that is relatively stable, which is advantageous for displacing oil.[76]

For the duration of the flooding trials, the Fars EOR Technology pressure gauge monitored the differential pressure. Figure 16 displays the differential pressure and recovery information for the individual core plugs C1, C2, C3, and C4. They were injected with HAP-NF until no more oil was produced, and then, a tertiary agent containing 0.1 wt % of NF was added at a continuous rate of 2 mL/min. Due to the two-phase flow that is taking place during the first 0.5 PV of brine inundation, a rise in differential pressure was noted. The differential pressure decreased and stabilized once brine breakthrough occurred. After 2 PV floods, no additional oil was produced, and the injection was halted. During the flooding, the differential pressure varied, but somehow it rose when NF was injected around 1.5 PV into this core plug. It is possible that some NPs adsorb, obstruct pore channels, and lower the permeability of core plugs as a result. The differential pressure of the various core plugs had a similar pattern since they are all from the same oil field. The little variation could be attributed to the slight difference in their permeabilities. Although many studies have shown that low salinity flooding boosts pressure and oil recovery,[34,70,77,78] absolute permeability on the other hand rises with salinity. Additionally, while oil viscosity (μo) stays constant, water viscosity (μw) increases proportionally to salinity. As a result, as salinity increases, the viscosity ratio ($\mu o/\mu w$) tends to decline, resulting in increased oil recovery.[12,79]

4. CONCLUSIONS

The impact of ionic strength on in situ functionalized HAP utilizing SDS for EOR was investigated in this work. The effects of HAP on sandstone wettability modification, IFT reduction between brine and oil,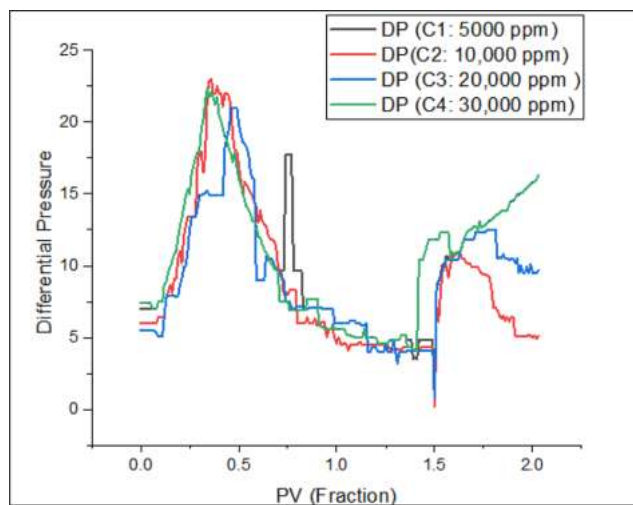 and oil displacement at high temperature and high pressure were studied. HAP reduced IFT, changed the wettability of sandstone rock from oil-wet to water-wet, and greatly improved oil recovery according to the results. The most significant inferences made from the findings are listed below.

1. The TEM and EDX data, as well as the free OH^- and PO_4^{3-} groups on the FTIR spectra and the XRD JCPDS-09430 HAP and crystallography, which influenced the property performance, all supported the hypothesis that HAP was synthesized.

2. Understanding of IFT reduction and dynamic wettability alteration was improved by using ZP measurements at various pH levels to understand HAP interactions. The TGA results also showed long-term stability in situations involving high temperatures.

3. Salinity affected IFT, wettability, and oil displacement; the ideal salinity for IFT and oil displacement was 30,000 ppm. However, there was a little increase in CA at 30,000 ppm. The small increase was still within the range of CA affected by NPs described in the literature. As a result, HAP seems suitable for usage during EOR operations in high-salinity reservoirs.

4. The IFT between oil and brine can be considerably reduced by surfactants to extremely low levels, which shows that SDS is the primary reason for the achieved IFT values. NP adsorption on rock surfaces has a significant impact on wettability. However, the improved oil recovery was eventually controlled by the presence of SDS and its effect on IFT, HAP's ability to adsorb on the surface of sandstone rocks and alter their wettability, and interactions between the ions of NaCl and the rock's permeability.

Table 2. Experimental Results for Oil Displacement

core sample	porosity (%)	permeability (mD)	initial oil saturation S_{oi} (%)	residual oil saturation S_{or} (%)	recovery using water flooding R_{WF} (%)	incremental oil recovery $R_{NP(NF)}$ (%)
C$_1$	22.3	275.001	80.6	20.4	64.37	6.3
C$_2$	21.2	243.369	69.5	19.14	45.67	11.5
C$_3$	23.5	274.698	84.8	11.74	69.98	15.3
C$_4$	25.3	395.101	88.4	19.88	62.17	17.9

AUTHOR INFORMATION

Corresponding Author

Mohd Zaidi Jaafar − *Departmentii of Petroleum Engineering, School of Chemical and Energy Engineering, Faculty of Engineering, Universiti Teknologi Malaysia, Johor Bahru 81310, Malaysia; Institute for Oil and Gas (IFOG), Universiti Technology Malaysia, 81310 Johor Bahru, Malaysia;* Email: mzaidi@utm.my/anam@utm.my

Authors

Eugene N. Ngouangna − *Departmentii of Petroleum Engineering, School of Chemical and Energy Engineering, Faculty of Engineering, Universiti Teknologi Malaysia, Johor Bahru 81310, Malaysia;* orcid.org/0000-0001-6068-2152

Mnam Norddin − *Departmentii of Petroleum Engineering, School of Chemical and Energy Engineering, Faculty of Engineering, Universiti Teknologi Malaysia, Johor Bahru 81310, Malaysia; Institute for Oil and Gas (IFOG), Universiti Technology Malaysia, 81310 Johor Bahru, Malaysia*

Augustine Agi − *Faculty of Chemical and Process Engineering Technology, University Malaysia Pahang, Kuantan, Pahang 68145, Malaysia*

Faruk Yakasai − *Departmentii of Petroleum Engineering, School of Chemical and Energy Engineering, Faculty of Engineering, Universiti Teknologi Malaysia, Johor Bahru 81310, Malaysia*

Jeffrey O. Oseh − *Departmentii of Petroleum Engineering, School of Chemical and Energy Engineering, Faculty of Engineering, Universiti Teknologi Malaysia, Johor Bahru 81310, Malaysia; Department of Petroleum Engineering, School of Engineering and Engineering Technology, Federal University of Technology, Owerri 460083 Imo State, Nigeria*

Stanley C. Mamah − *Advanced Membrane Technology Research Centre (AMTEC), School of Chemical and Energy Engineering, Faculty of Engineering, Universiti Teknologi Malaysia, Skudai 81310 Johor, Malaysia*

Muftahu N. Yahya − *Departmentii of Petroleum Engineering, School of Chemical and Energy Engineering, Faculty of Engineering, Universiti Teknologi Malaysia, Johor Bahru 81310, Malaysia*

Muhanad Al-Ani − *Departmentii of Petroleum Engineering, School of Chemical and Energy Engineering, Faculty of Engineering, Universiti Teknologi Malaysia, Johor Bahru 81310, Malaysia*

Complete contact information is available at:
https://pubs.acs.org/10.1021/acsomega.3c00695

Notes

The authors declare no competing financial interest.

REFERENCES

(1) Addison, T.; Roe, A.; Stevens, P. *4 The Role of Oil and Gas in the Economic Development of the Global Economy*; Oxford University Press, 2018.

(2) Li, M.; Li, L.; Strielkowski, W. *The Impact of Urbanization and Industrialization on Energy Security: A Case Study of China*; MDPI, 2019; 1−22, No. i.

(3) Gielen, D.; Boshell, F.; Saygin, D.; Bazilian, M. D.; Wagner, N.; Gorini, R. The Role of Renewable Energy in the Global Energy Transformation. *Energy Strategy Rev.* **2019**, *24*, 38−50.

(4) Muggeridge, A.; Cockin, A.; Webb, K.; Frampton, H.; Collins, I.; Moulds, T.; Salino, P. Recovery Rates, Enhanced Oil Recovery and Technological Limits. *Phil. Trans. Math. Phys. Eng. Sci.* **2014**, *372*, 20120320.

(5) Yu, S.; Wu, J.; Wang, M.; Shi, W.; Xia, G.; Jia, J.; Kang, Z.; Han, D. Haplotype Variations in QTL for Salt Tolerance in Chinese Wheat Accessions Identified by Marker-Based and Pedigree-Based Kinship Analyses. *Crop J.* **2020**, *8*, 1011−1024.

(6) van der Spek, D.; van Arendonk, J.; Bovenhuis, H. Genome-Wide Association Study for Claw Disorders and Trimming Status in Dairy Cattle. *J. Dairy Sci.* **2015**, *98*, 1286−1295.

(7) Razavirad, F.; Shahrabadi, A.; Dehkordi, P. B.; Rashidi, A. Experimental Pore-Scale Study of a Novel Functionalized Iron-Carbon Nanohybrid for Enhanced Oil Recovery (EOR). *Nanomaterials* **2022**, *12*, 103.

(8) Gbadamosi, A. O.; Junin, R.; Manan, M. A.; Agi, A.; Yusuff, A. S. An Overview of Chemical Enhanced Oil Recovery: Recent Advances and Prospects. *Int. Nano Lett.* **2019**, *9*, 171−202.

(9) Ngouangna, E. N.; Manan, M. A.; Oseh, J. O.; Norddin, M. N. A. M.; Agi, A.; Gbadamosi, A. O. Influence of (3−Aminopropyl) Triethoxysilane on Silica Nanoparticle for Enhanced Oil Recovery. *J. Mol. Liq.* **2020**, *315*, 113740.

(10) Thomas, S. Enhanced Oil Recovery − An Overview. *Oil Gas Sci. Technol.* **2008**, *63*, 9−19.

(11) Agi, A.; Junin, R.; Gbadamosi, A.; Manan, M.; Jaafar, M. Z.; Abdullah, M. O.; Arsad, A.; Azli, N. B.; Abdurrahman, M.; Yakasai, F. Comparing Natural and Synthetic Polymeric Nanofluids in a Mid-Permeability Sandstone Reservoir Condition. *J. Mol. Liq.* **2020**, *317*, 113947.

(12) Joshi, D.; Maurya, N. K.; Kumar, N.; Mandal, A. Experimental Investigation of Silica Nanoparticle Assisted Surfactant and Polymer Systems for Enhanced Oil Recovery. *J. Petrol. Sci. Eng.* **2022**, *216*, 110791.

(13) Jouenne, S. Polymer Flooding in High Temperature, High Salinity Conditions: Selection of Polymer Type and Polymer Chemistry, Thermal Stability. *J. Petrol. Sci. Eng.* **2020**, *195*, 107545.

(14) Ghosh, P.; Mohanty, K. K. Study of Surfactant-Polymer Flooding in High Temperature High Salinity Carbonate Rocks Study of Surfactant-Polymer Flooding in High Temperature High Salinity. *Energy Fuels* **2019**, *33*, 4130−4145.

(15) Belhaj, A. F.; Elraies, K. A.; Mahmood, S. M.; Zulkifli, N. N.; Akbari, S.; Hussien, O. S. The Effect of Surfactant Concentration , Salinity , Temperature , and PH on Surfactant Adsorption for Chemical Enhanced Oil Recovery : A Review. *J. Pet. Explor. Prod. Technol.* **2020**, *10*, 125−137.

(16) Maurya, N. K.; Mandal, A. Investigation of synergistic effect of nanoparticle and surfactant in macro emulsion based EOR application in oil reservoirs. *Chem. Eng. Res. Des.* **2018**, *132*, 370−384.

(17) Manshad, A. K.; Rezaei, M.; Moradi, S.; Nowrouzi, I.; Mohammadi, A. H. Wettability alteration and interfacial tension (IFT) reduction in enhanced oil recovery (EOR) process by ionic liquid flooding. *J. Mol. Liq.* **2017**, *248*, 153−162.

(18) Imuetinyan, H.; Agi, A.; Gbadamosi, A.; Junin, R.; Oseh, J. Oil-Water Interfacial Tension , Wettability Alteration and Foaming Studies of Natural Surfactant Extracted from Vernonia Amygdalina. *Pet. Res.* **2022**, *7*, 350−356.

(19) Sheng, J. J. Status of Surfactant EOR Technology. *Petroleum* **2015**, *1*, 97−105.

(20) Eltoum, H.; Yang, Y. L.; Hou, J. R. The Effect of Nanoparticles on Reservoir Wettability Alteration: A Critical Review. *Pet. Sci.* **2021**, *18*, 136−153.

(21) Agi, A.; Junin, R.; Gbadamosi, A.; Manan, M.; Jaafar, M. Z.; Abdullah, M. O.; Arsad, A.; Azli, N. B.; Abdurrahman, M.; Yakasai, F.

Comparing Natural and Synthetic Polymeric Nanofluids in a Mid-Permeability Sandstone Reservoir Condition. *J. Mol. Liq.* **2020**, *317*, 113947.

(22) Yakasai, F.; Jaafar, M. Z.; Bandyopadhyay, S.; Agi, A. Current Developments and Future Outlook in Nanofluid Flooding: A Comprehensive Review of Various Parameters Influencing Oil Recovery Mechanisms. *J. Ind. Eng. Chem.* **2021**, *93*, 138−162.

(23) Agista, M. N.; Guo, K.; Yu, Z. A State-of-the-Art Review of Nanoparticles Application in Petroleum with a Focus on Enhanced Oil Recovery. *Appl. Sci.* **2018**, *8*, 871.

(24) Khan, M. I.; Islam, M. R. Enhanced Oil Recovery (EOR) Operations. *The Petroleum Engineering Handbook: Sustainable Operations*; Elsevier, 2007; pp 243−293, No. November.

(25) Agi, A.; Junin, R.; Gbadamosi, A. Mechanism Governing Nanoparticle Flow Behaviour in Porous Media: Insight for Enhanced Oil Recovery Applications. *Int. Nano Lett.* **2018**, *8*, 49−77.

(26) Behzadi, A.; Mohammadi, A. Environmentally Responsive Surface-Modified Silica Nanoparticles for Enhanced Oil Recovery. *J. Nanopart. Res.* **2016**, *18*, 266.

(27) Sepehri, M.; Moradi, B.; Emamzadeh, A.; Mohammadi, A. H. Experimental Study and Numerical Modeling for Enhancing Oil Recovery from Carbonate Reservoirs by Nanoparticle Flooding. *J. Nanopart. Res.* **2019**, *74*, 5.

(28) Mondal, S.; Mondal, A.; Mandal, N.; Mondal, B.; Mukhopadhyay, S. S.; Dey, A.; Singh, S. Physico-Chemical Characterization and Biological Response of Labeo Rohita-Derived Hydroxyapatite Scaffold. *Bioprocess Biosyst. Eng.* **2014**, *37*, 1233−1240.

(29) Ali, J. A.; Kolo, K.; Manshad, A. K.; Mohammadi, A. H. Recent Advances in Application of Nanotechnology in Chemical Enhanced Oil Recovery: Effects of Nanoparticles on Wettability Alteration, Interfacial Tension Reduction, and Flooding. *Egypt. J. Pet.* **2018**, *27*, 1371−1383.

(30) Mamah, S. C.; Goh, P. S.; Ismail, A. F.; Yogarathinam, L. T.; Suzaimi, N. D.; Opia, A. C.; Ojo, S.; Ngwana, N. E. Bio-Polymer Modified Nanoclay Embedded Forward Osmosis Membranes with Enhanced Desalination Performance. *J. Appl. Polym. Sci.* **2022**, *139*, No. e52473.

(31) Toma, S. H.; Santos, J. J.; da Silva, D. G.; Huila, M. F. G.; Toma, H. E.; Araki, K. Improving stability of iron oxide nanofluids for enhanced oil recovery: Exploiting wettability modifications in carbonaceous rocks. *J. Petrol. Sci. Eng.* **2022**, *212*, 110311.

(32) Hendraningrat, L.; Li, S. SPE 164106 A Coreflood Investigation of Nanofluid Enhanced Oil Recovery in Low- Medium Permeability Berea Sandstone. *SPE International Symposium on Oilfield Chemistry*; OnePetro, 2013.

(33) Joshi, D.; Maurya, N. K.; Kumar, N.; Mandal, A. Experimental Investigation of Silica Nanoparticle Assisted Surfactant and Polymer Systems for Enhanced Oil Recovery. *J. Petrol. Sci. Eng.* **2022**, *216*, 110791.

(34) Austad, T.; Rezaeidoust, A.; Puntervold, T. SPE 129767 Chemical Mechanism of Low Salinity Water Flooding in Sandstone Reservoirs. *SPE Improved Oil Recovery Symposium*; OnePetro, 2010.

(35) Aghaeifar, Z.; Strand, S.; Puntervold, T. Signi Fi Cance of Capillary Forces during Low-Rate Water Fl Ooding. *Energy Fuels* **2019**, *33*, 3989−3997.

(36) Nourani, M.; Tichelkamp, T.; Hosseinzade Khanamiri, H.; Johansen, T.; Karlsen Hov, I.; Gaweł, B.; Torsæter, O.; Øye, G.; Øye, G. Dynamic Wettability Alteration for Combined Low Salinity Brine Injection and Surfactant Flooding on Silica Surface. *SN Appl. Sci.* **2020**, *2*, 1274−1313.

(37) Ngouangna, E. N.; Zaidi Jaafar, M.; Norddin, M. N. A. M.; Agi, A.; Oseh, J. O.; Mamah, S. Surface Modification of Nanoparticles to Improve Oil Recovery Mechanisms: A Critical Review of the Methods, Influencing Parameters, Advances and Prospects. *J. Mol. Liq.* **2022**, *360*, 119502.

(38) Predoi, D.; Iconaru, S. L.; Predoi, M. V. Fabrication of silver-and zinc-doped hydroxyapatite coatings for enhancing antimicrobial effect. *Coatings* **2020**, *10*, 905.

(39) Ngouangna, E. N.; Jaafar, M. Z.; Norddin, M. N. A. M.; Agi, A.; Risal, A. R.; Mamah, S. C.; Oseh, J. O. The Effect of Hydroxyapatite

Nanoparticles on Wettability and Brine-Oil Interfacial Tension as Enhance Oil Recovery Mechanisms. *J. Petrol. Sci. Eng.* **2022**, *218*, 110941.

(40) Chakravarty, M.; Vora, A. Nanotechnology-based antiviral therapeutics. *Drug Deliv Transl Res.* **2021**, *11* (3), 748−787.

(41) Babakhani, P. The Impact of Nanoparticle Aggregation on Their Size Exclusion during Transport in Porous Media : One- and Three-Dimensional Modelling Investigations. *Sci. Rep.* **2019**, *9*, 14071.

(42) Chakraborty, S.; Panigrahi, P. K. Stability of Nano Fl Uid : A Review. *Appl. Therm. Eng.* **2020**, *174*, 115259.

(43) Varadarajan, V.; Varsha, M.; Vijayasekaran, K. Comparative Studies of Hydroxyapatite (HAp) Nanoparticles Synthesized by Using Different Green Templates Comparative Studies of Hydroxyapatite (HAp) Nanoparticles Synthesized by Using Different Green Templates. *AIP Conf.* **2020**, *2240*, 080002.

(44) Müller, K. H.; Motskin, M.; Philpott, A. J.; Routh, A. F.; Shanahan, C. M.; Duer, M. J.; Skepper, J. N. The effect of particle agglomeration on the formation of a surface-connected compartment induced by hydroxyapatite nanoparticles in human monocyte-derived macrophages. *Biomaterials* **2014**, *35*, 1074−1088.

(45) Kumar, G.; Behera, U. S.; Mani, E.; Sangwai, J. S. Engineering the Wettability Alteration of Sandstone Using Surfactant-Assisted Functional Silica Nano Fl Uids in Low-Salinity Seawater for Enhanced Oil Recovery. *ACS Eng. Au* **2022**, *2*, 421−435.

(46) Padmanabhan, V. P.; Sankara Narayanan, T. S. N.; Sagadevan, S. Advanced Lithium Substituted Hydroxyapatite Nanoparticles for Antimicrobial and Hemolytic Studies. *New J. Chem.* **2019**, *43*, 18484−18494.

(47) Kaygili, O.; Keser, S.; Bulut, N.; Ates, T. Physica B : Condensed Matter Characterization of Mg-Containing Hydroxyapatites Synthesized by Combustion Method. *Phys. B* **2018**, *537*, 63−67.

(48) Tariq, U.; Haider, Z.; Tun, U.; Onn, H.; Ali, J. Determination of Calcium to Phosphate Ratio in Hydroxyapatite Extracted from Bovine Bone Using LIBS. *Bul. Opt.* **2016**, *2*, 48−53.

(49) Zainuddin, D. U.; Dachlan, A.; Kazakov, A. L.; Kuznetsov, P. A.; Lempert, A. A.; Kartika, I. Calcium to Phosphate Ratio Measurements in Calcium Phosphates Using LIBS Calcium to Phosphate Ratio Measurements in Calcium Phosphates Using LIBS. **2018**.

(50) Chandrasekar, A.; Sagadevan, S.; Dakshnamoorthy, A. Synthesis and Characterization of Nano-Hydroxyapatite (n-HAP) Using the Wet Chemical Technique. *Int. J. Phys. Sci.* **2013**, *8*, 1639−1645.

(51) Padmanabhan, V. P.; Kulandaivelu, R.; Santhana Panneer, D.; Vivekananthan, S.; Sagadevan, S.; Anita Lett, J. Microwave Synthesis of Hydroxyapatite Encumbered with Ascorbic Acid Intended for Drug Leaching Studies. *Mater. Res. Innovations* **2020**, *24*, 171−178.

(52) Bouropoulos, N.; Stampolakis, A.; Mouzakis, D. E. Dynamic Mechanical Properties of Calcium Alginate-Hydroxyapatite Nanocomposite Hydrogels. *Sci. Adv. Mater.* **2010**, *2*, 239−242.

(53) Liao, C. J.; Lin, F. H.; Chen, K. S.; Sun, J. S. Thermal Decomposition and Reconstitution of Hydroxyapatite in Air Atmosphere. *Biomaterials* **1999**, *20*, 1807−1813.

(54) N Jagadale, P.; P Jagtap, P.; G Joshi, M.; R Bamane, S. A Prototype Synthesis and Characterization of Hydroxyapatite Bioceramics Nanocrystallites. *Adv. Mater. Lett.* **2016**, *7*, 325−329.

(55) Pillai, P.; Saw, R. K.; Singh, R.; Padmanabhan, E.; Mandal, A. Effect of synthesized lysine-grafted silica nanoparticle on surfactant stabilized O/W emulsion stability: Application in enhanced oil recovery. *J. Petrol. Sci. Eng.* **2019**, *177*, 861−871.

(56) Abdullah, M. M. S.; Al-lohedan, H. A. Novel Bio-Based Amphiphilic Ionic Liquids for the Efficient Demulsification of Heavy Crude Oil Emulsions. **2021**.

(57) Fan, H.; Striolo, A. Nanoparticle Effects on the Water-Oil Interfacial Tension. *Phys. Rev. E: Stat., Nonlinear, Soft Matter Phys.* **2012**, *86*, 051610.

(58) Esfandiarian, A.; Azdarpour, A.; Santos, R. M.; Mohammadian, E.; Hamidi, H.; Sedaghat, M.; Dehkordi, P. B. Mechanistic Investigation of LSW/Surfactant/Alkali Synergism for Enhanced Oil Recovery : Fluid − Fluid Interactions Mechanistic Investigation of LSW/

Surfactant/Alkali Synergism for Enhanced Oil Recovery : Fluid − Fluid Interactions. *ACS Omega* **2020**, *5*, 30059−30072.

(59) Mohajeri, M.; Reza Rasaei, M.; Hekmatzadeh, M. Experimental Study on Using SiO2 Nanoparticles along with Surfactant in an EOR Process in Micromodel. *Pet. Res.* **2019**, *4*, 59−70.

(60) Kedar, V.; Bhagwat, S. S. Effect of Salinity on the IFT between Aqueous Surfactant Solution and Crude Oil. *Pet. Sci. Technol.* **2018**, *36*, 835−842.

(61) Jiravivitpanya, J.; Maneeintr, K.; Boonpramote, T. Experiment on Measurement of Interfacial Tension for Subsurface Conditions of Light Oil from Thailand. **2017**, 18007.

(62) Mgcl, D.; Salts, M.; Tension, I.; Behera, U. S.; Sangwai, J. S. Synergistic Effect of Brine System Containing Mixed Monovalent (NaCl , KCl) Synergistic E Ff Ect of Brine System Containing Mixed Monovalent (NaCl , KCl) and Divalent (MgCl 2 , MgSO 4) Salts on the Interfacial Tension of Pure Hydrocarbon − Brine Sys. *Energy Fuels* **2020**, *34*, 4201−4212.

(63) Ngo, I.; Sasaki, K.; Nguele, R.; Sugai, Y. Formation Damage Induced by Water-Based Alumina Nano Fl Uids during Enhanced Oil Recovery : In Fl Uence of Post Fl Ush Salinity. *ACS Omega* **2020**, *5*, 27103−27112.

(64) Safarzadeh, S.; Bila, A.; Torsæter, O. Experimental Investigation of the Effect of Silica Nanoparticles on Interfacial Tension and Wettability during Low Salinity Water Flooding. A Micromodel Study. *J. Mod. Nanotechnol.* **2022**, *2*, 1−19.

(65) Brown, M. A.; Goel, A.; Abbas, Z. Electrical Double Layer Effect of Electrolyte Concentration on the Stern Layer Thickness at a Charged Interface Angewandte. **2016**, 3790−3794. DOI: 10.1002/anie.201512025.

(66) Li, Y.; Girard, M.; Shen, M.; Millan, J. A.; Olvera de la Cruz, M.; Cruz, D. Strong Attractions and Repulsions Mediated by Monovalent Salts. *Proc. Natl. Acad. Sci. U.S.A.* **2017**, *114*, 11838−11843.

(67) Pal, N.; Verma, A.; Ojha, K.; Mandal, A. Nanoparticle-Modi Fi Ed Gemini Surfactant Foams as Ef Fi Cient Displacing Fl Uids for Enhanced Oil Recovery. *J. Mol. Liq.* **2020**, *310*, 113193.

(68) Al-anssari, S.; Wang, S.; Barifcani, A.; Lebedev, M.; Iglauer, S. Effect of Temperature and SiO 2 Nanoparticle Size on Wettability Alteration of Oil-Wet Calcite. *Fuel* **2017**, *206*, 34−42.

(69) Mahanta, K. K.; Mishra, G. C.; Kansal, M. L. Estimation of the electric double layer thickness in the presence of two types of ions in soil water. *Appl. Clay Sci.* **2014**, *87*, 212−218.

(70) Xie, Q.; Liu, F.; Chen, Y.; Yang, H.; Saeedi, A.; Hossain, M. M. Effect of electrical double layer and ion exchange on low salinity EOR in a pH controlled system. *J. Petrol. Sci. Eng.* **2019**, *174*, 418−424.

(71) Firoozabadi, A. Hydrophobic Hydration and the E Ff Ect of NaCl Salt in the Adsorption of Hydrocarbons and Surfactants on Clathrate Hydrates. *ACS Cent. Sci.* **2018**, *4*, 820−831.

(72) Endo, S.; Pfennigsdorff, A.; Goss, K. Salting-Out Effect in Aqueous NaCl Solutions: Trends with Size and Polarity of Solute Molecules. *Environ. Sci. Technol.* **2012**, *46*, 1496−1503.

(73) Grundl, G.; Müller, M.; Touraud, D.; Kunz, W. S. C. Salting-out and salting-in effects of organic compounds and applications of the salting-out effect of Pentasodium phytate in different extraction processes. *J. Mol. Liq.* **2017**, *236*, 368−375.

(74) Petersen, P. B.; Saykally, R. J. Adsorption of Ions to the Surface of Dilute Electrolyte Solutions : The Jones - Ray Effect Revisited. *J. Am. Chem. Soc.* **2005**, *127*, 15446−15452.

(75) Ruiz-agudo, E.; Urosevic, M.; Putnis, C. V.; Rodríguez-navarro, C.; Cardell, C.; Putnis, A. Ion-Speci Fi c Effects on the Kinetics of Mineral Dissolution. *Chem. Geol.* **2011**, *281*, 364−371.

(76) Yang, Y.; Cheng, T.; Wu, H.; You, Z.; Shang, D.; Hou, J. Enhanced Oil Recovery Using Oleic Acid-Modified Titania Nanofluids : Underlying Mechanisms and Oil-Displacement Performance Enhanced Oil Recovery Using Oleic Acid-Modified Titania Nanofluids : Underlying Mechanisms and Oil-Displacement. *Energy Fuels* **2020**, *34*, 5813−5822.

(77) Al-Saedi, H. N.; Alhuraishawy, A. K.; Flori, R.; Brady, P. V. Sequential Injection Mode of High - Salinity/Low - Salinity Water in

Sandstone Reservoirs : Oil Recovery and Surface Reactivity Tests. *J. Pet. Explor. Prod. Technol.* **2019**, *9*, 261−270.

(78) Xie, Q.; Liu, F.; Chen, Y.; Yang, H.; Saeedi, A.; Hossain, M. M. Effect of electrical double layer and ion exchange on low salinity EOR in a pH controlled system. *J. Petrol. Sci. Eng.* **2019**, *174*, 418−424.

(79) Mohammad Salehi, M.; Omidvar, P.; Naeimi, F. Salinity of Injection Water and Its Impact on Oil Recovery Absolute Permeability , Residual Oil Saturation , Interfacial Tension and Capillary Pressure. *Egypt. J. Pet.* **2017**, *26*, 301−312.